

Gravitational Lensing by Charged Accelerating Black Holes

Torben C. Frost

*ZARM, University of Bremen, 28359 Bremen, Germany and Institute for Theoretical Physics,
Leibniz University Hannover, 30167 Hannover, Germany
E-mail: torben.frost@zarm.uni-bremen.de*

Current astrophysical observations show that on large scale the Universe is electrically neutral. However, locally this may be quite different. Black holes enveloped by a plasma in the presence of a strong magnetic field may have acquired a significant electric charge. We can also expect that some of these charged black holes are moving. Consequently to describe them we need spacetime metrics describing moving black holes. In general relativity such a solution is given by the charged C-de Sitter-metric. In this article we will assume that it can be used to describe moving charged black holes. We will investigate how to observe the electric charge using gravitational lensing. First we will use elliptic integrals and functions to solve the geodesic equations. Then we will derive lens equation, travel time and redshift. We will discuss the impact of the electric charge on these observables and potential limitations for its observation.

Keywords: Black Holes; Gravitational Lensing

1. Introduction

X-ray and gravitational wave observations indicate that stellar mass black holes are widely distributed in our galaxy.^{1,2} In addition, the motion of gas and stars^{3,4} around galactic centres as well as the recent observation of the shadow of the compact object in the centre of the galaxy M87⁵ indicate that in the centre of most galaxies we can find at least one supermassive black hole (SMBH). While the resolution of these observations are not yet precise enough to exclude all alternative theories of gravity or different types of compact objects all observational features indicate that these compact objects can be described either by the Schwarzschild metric or the Kerr metric.

Concurrent astrophysical observations show that our Universe is electrically neutral. This indicates that all astrophysical objects, among them black holes, do not carry a significant electric charge. However, if a black hole is surrounded by a plasma with sufficiently large magnetic fields, the black hole may acquire a significant electric charge.⁶ In general relativity charged black holes that are at rest and do not carry a spin are described by the Reissner-Nordström metric, or, if we want to take the cosmological expansion into account, by the Reissner-Nordström-de Sitter metric. In the case that we consider real astrophysical environments it is very unlikely that black holes are at rest. Instead it is more realistic to assume that they constantly undergo accelerated motion. Consequently we need spacetimes describing accelerating black holes to describe them accurately. In the framework of general relativity a family of such solutions is described by the charged C-de Sitter metric.⁷ The metric

is an exact solution to Einstein's electrovacuum field equations with cosmological constant. It generalises the Reissner-Nordström-de Sitter metric by introducing the acceleration parameter α in addition to the mass parameter m , the electric charge e and the cosmological constant Λ . The charged C-de Sitter metric is axisymmetric and static and describes a charged accelerating black hole with cosmological constant. The acceleration of the black hole results from conical singularities on the axes, which are commonly interpreted as a string pulling the black hole and a strut pushing the black hole. These conical singularities make the spacetime on a first view appear unphysical. However, it may still serve as an approximation for black holes undergoing accelerated motion. Gravitational lensing in the C-metric only attracted attention relatively recently. Grenzebach, Perlick and Lämmerzahl^{8,9} investigated the shadow of accelerating black holes in the whole Plebański-Demiański family with acceleration.¹⁰ Sharif and Iftikhar¹¹ calculated the deflection angle for light rays in the equatorial plane for accelerating Kerr-NUT black holes. The method they used explicitly assumes that the light rays are located in the equatorial plane of the spacetime. However, Alrais Alawadi, Batic and Nowakowski¹² and subsequently Frost and Perlick¹³ demonstrated that the C-metric possesses a photon cone $\vartheta_{\text{ph}} \neq \pi/2$ and therefore the method of Sharif and Iftikhar cannot be directly applied. Alrais Alawadi, Batic and Nowakowski¹² calculated the deflection angle on the photon cone. Only a short time later Frost and Perlick¹³ investigated gravitational lensing in the C-metric. In their work Frost and Perlick¹³ used the canonical form of the elliptic integrals and Jacobi's elliptic functions to solve the geodesic equations. Then, following the approach of Grenzebach, Perlick and Lämmerzahl,⁸ they fixed an observer in the region of outer communication and introduced an orthonormal tetrad to relate latitude and longitude on the observer's celestial sphere to the constants of motion of the light rays. Using the conventions in Bohn et al.¹⁴ they formulated a lens equation, they derived the redshift and the travel time of individual light rays on the celestial sphere of the observer. In this article we will extend their approach to the charged C-de Sitter metric. For this purpose the remainder of this article is structured as follows. As not all readers may be familiar with the charged C-de Sitter metric we will provide a short overview of its physical properties in Section 2. In Section 3 we will demonstrate how to solve the equations of motion. In Section 4 we will first introduce the orthonormal tetrad and show how to parameterise the light rays using the angles on the observer's celestial sphere. Then we will introduce the lens map, formulate the lens equation, and calculate the redshift and the travel time of light rays. In Section 5 we will shortly summarise our results and conclusions. Throughout the whole article we will use geometric units with $c = G = 1$. The metric signature is chosen as $(-, +, +, +)$.

2. The Charged C-de Sitter-Metric

The charged C-de Sitter metric is a solution to Einstein's electrovacuum field equations with cosmological constant. It belongs to the Plebański-Demiański family of

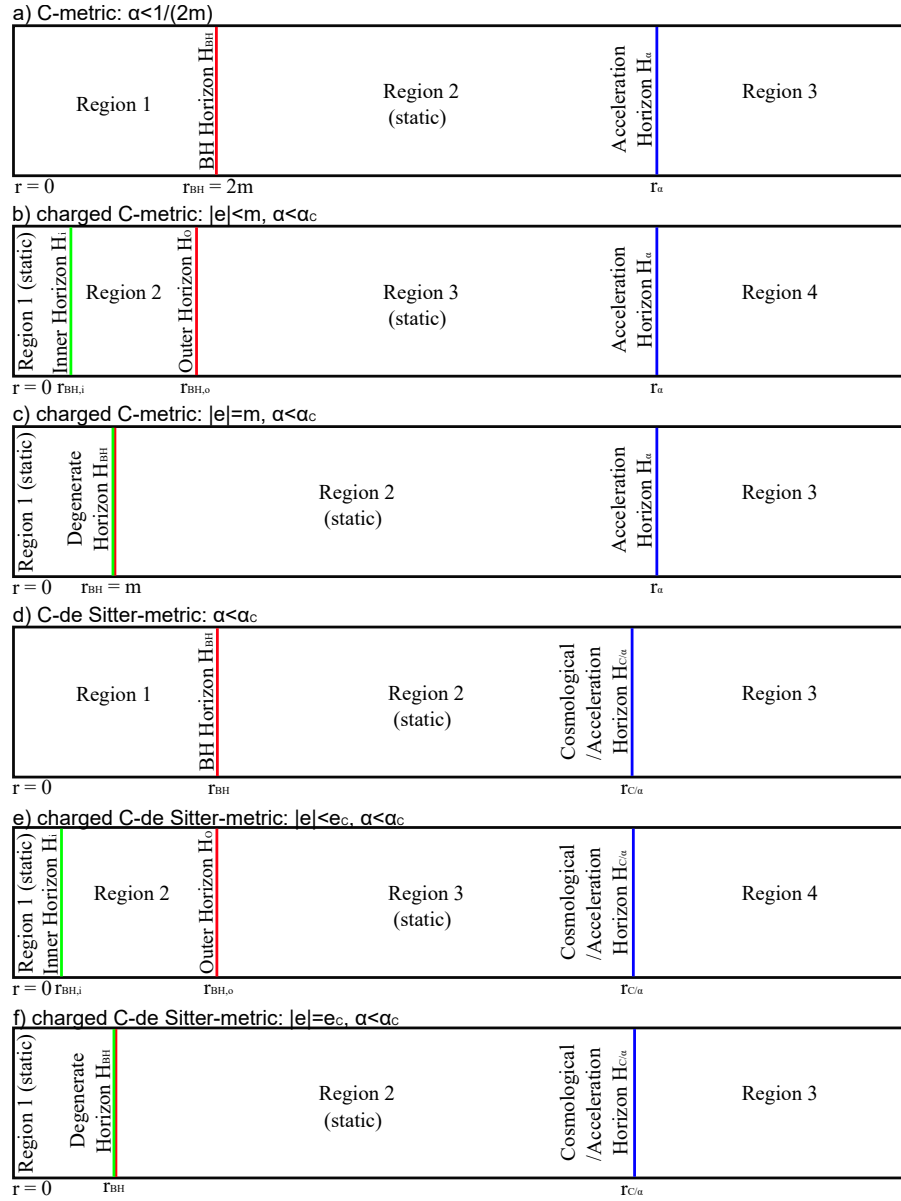


Fig. 1. Position of the curvature singularity at $r = 0$ and the coordinate singularities in a) the C-metric, the charged C-metric with b) $|e| < m$ and c) $|e| = m$, d) the C-de Sitter metric and the charged C-de Sitter metric with e) $|e| < e_c$ and f) $|e| = e_c$. Note that the angular coordinates are suppressed and other singularities are not shown.

spacetimes of Petrov type D¹⁰ and is axisymmetric and static. The spacetime is characterised by four parameters: the mass parameter m , the electric charge e , the cosmological constant Λ , and the acceleration parameter α . Its line element reads⁷

$$g_{\mu\nu}dx^\mu dx^\nu = \frac{1}{\Omega(r, \vartheta)^2} \left(-Q(r)dt^2 + \frac{dr^2}{Q(r)} + \frac{r^2 d\vartheta^2}{P(\vartheta)} + r^2 \sin^2 \vartheta P(\vartheta) d\varphi^2 \right), \quad (1)$$

where

$$Q(r) = (1 - \alpha^2 r^2) \left(1 - \frac{2m}{r} + \frac{e^2}{r^2} \right) - \frac{\Lambda}{3} r^2, \quad (2)$$

$$P(\vartheta) = 1 - 2\alpha m \cos \vartheta + \alpha^2 e^2 \cos^2 \vartheta, \quad (3)$$

$$\Omega(r, \vartheta) = 1 - \alpha r \cos \vartheta. \quad (4)$$

When we set $\alpha = 0$ the metric reduces to the Reissner-Nordström-de Sitter family of spacetimes including the Schwarzschild metric ($e = 0$, $\Lambda = 0$), the Reissner-Nordström metric ($\Lambda = 0$), and the Schwarzschild-de Sitter metric ($e = 0$). For $e = 0$ and $\Lambda = 0$ the metric reduces to the regular C-metric. For $e = 0$ it reduces to the C-de Sitter metric and for $\Lambda = 0$ it reduces to the charged C-metric. In accordance with observations we choose $0 < m$. Theoretically the electric charge e can take any real value but because the line element (1) only contains its square we restrict it such that we have $0 \leq e \leq e_C$. Because we live in an expanding Universe we will assume that $0 \leq \Lambda < \Lambda_C$. α can be restricted from the symmetry of the spacetime. When we replace α by $-\alpha$ and substitute $\vartheta \rightarrow \pi - \vartheta$ we see that (1) is invariant and consequently we can restrict the acceleration parameter to $0 < \alpha < \alpha_C$. Here, e_C , Λ_C and α_C are critical parameters that have to be chosen according to the desired interpretation of the spacetime. In the charged C-de Sitter metric the time coordinate t can assume any real value. In addition we choose the angular coordinates ϑ and φ such that they represent the angular coordinates on the two sphere S^2 . The range of the r coordinate is determined by the singularity structure of the spacetime, in particular the singularities arising from $Q(r)$ and $\Omega(r, \vartheta)$. We will discuss these singularities and their implications for the r coordinate in the following. The spacetime admits several singularities. We start by discussing the singularities arising from $Q(r)$. In total $Q(r)$ can lead to up to five singularities in the metric. The equation $Q(r) = 0$ can lead to up to four singularities. In addition the metric has another singularity at $r = 0$. The singularity at $r = 0$ is a curvature singularity. For $e \neq 0$ the curvature singularity is timelike. Because lightlike and timelike geodesics cannot cross the curvature singularity particle motion is limited to $0 < r$. In addition the conformal factor becomes singular when $\Omega(r, \vartheta) = 0$. This singularity corresponds to conformal infinity and limits the radius coordinate r . The singularity starts at $r = 1/\alpha$ on the axis $\vartheta = 0$ and extends to $r = \infty$ for $\pi/2 \leq \vartheta$. The other singularities are only coordinate singularities r_H that can be removed using appropriate coordinate transformations (for the C-metric the procedure is demonstrated in Ref. 15). In

this article we restrict to black hole spacetimes and consequently all coordinate singularities with $0 < r_H$ are horizons. In general the horizon structure of each metric depends on the parameters of the spacetime. For each spacetime the critical parameters e_C , Λ_C and α_C have to be chosen such that all horizons are real and that they lead to physically meaningful black hole spacetimes. The horizon structure of the whole family of charged C-de Sitter metrics is shown in Fig. 1. Panel a) shows the horizon structure of the C-metric. The C-metric has two horizons, a black hole horizon at $r_{\text{BH}} = 2m$ and an acceleration horizon at $r_{\text{BH}} < r_\alpha = 1/\alpha$. Between the horizons the spacetime is static. In the other two regions the spacetime is non-static. Panels b) and c) show the horizon structure for the charged C-metric. The main difference to the C-metric is that the spacetime now contains an inner and an outer black hole horizon $r_{\text{BH},i} \leq r_{\text{BH},o} < r_\alpha$. When $e = m$ both horizons coincide and form a degenerate horizon at $r_{\text{BH}} = m$. The regions $0 < r < r_{\text{BH},i}$ and $r_{\text{BH},o} < r < r_\alpha$ are static. The other two regions are non-static. When we include the cosmological constant Λ (panels d) to f)) the radius coordinates of the horizons change, however, the horizon structure remains unchanged. For a more detailed discussion of the horizon structure in the C-metric we refer the interested reader to Ref. 13. In our case we always choose e_C such that $P(\vartheta)$ does not lead to singularities in the metric. Finally, the spacetime has two singularities on the axes at $\sin \vartheta = 0$. As demonstrated in Refs. 7 and 15 these singularities are conical singularities. They are associated with a deficit angle ($\vartheta = 0$) and a surplus angle ($\vartheta = \pi$). The charged C-de Sitter metric is usually interpreted such that it describes a charged accelerating black hole with cosmological constant. In its full analytic extension the spacetime describes two causally separated charged black holes accelerating away from each other. The conical singularity at $\vartheta = 0$ is commonly interpreted as a string pulling the black hole, while the conical singularity at $\vartheta = \pi$ is interpreted as a strut pushing the black hole. As demonstrated in Ref. 7 and 15 one of the conical singularities can always be removed, however, as in our previous work¹³ here we will retain both singularities to show the effects of both, the string and the strut on geodesic motion.

3. Equations of Motion

In the charged C-de Sitter metric the equations of motion for light rays are fully separable. In Mino parameterisation¹⁶ they read^{8,13}

$$\frac{dt}{d\lambda} = \frac{r^2 E}{Q(r)}, \quad (5)$$

$$\left(\frac{dr}{d\lambda}\right)^2 = E^2 r^4 - r^2 Q(r) K, \quad (6)$$

$$\left(\frac{d\vartheta}{d\lambda}\right)^2 = P(\vartheta) K - \frac{L_z^2}{\sin^2 \vartheta}, \quad (7)$$

$$\frac{d\varphi}{d\lambda} = \frac{L_z}{\sin^2 \vartheta P(\vartheta)}, \quad (8)$$

where the Mino parameter λ is related to the affine parameter s by

$$\frac{d\lambda}{ds} = \frac{\Omega(r, \vartheta)^2}{r^2}. \quad (9)$$

Here, the three constants of motion E , L_z and K are the energy, the angular momentum about the z axis and the Carter constant of the light ray, respectively. In this article we choose the energy E such that $dt/d\lambda > 0$. In the following we will briefly discuss the equations of motion, the turning points of the r and the ϑ motion and identify the locations of the photon sphere and the photon cone. Then we will turn to solving the equations of motion. We will derive the solutions to the equations of motion for arbitrary initial conditions $(x_i^\mu) = (x^\mu(\lambda_i)) = (t_i, r_i, \vartheta_i, \varphi_i)$ closely following the procedures described in Refs. 13 and 17. Because the main focus of this article will be to apply our results to gravitational lensing we will limit our discussion to lightlike geodesics in the region of outer communication between photon sphere and the cosmological/acceleration horizon.

3.1. The r Motion

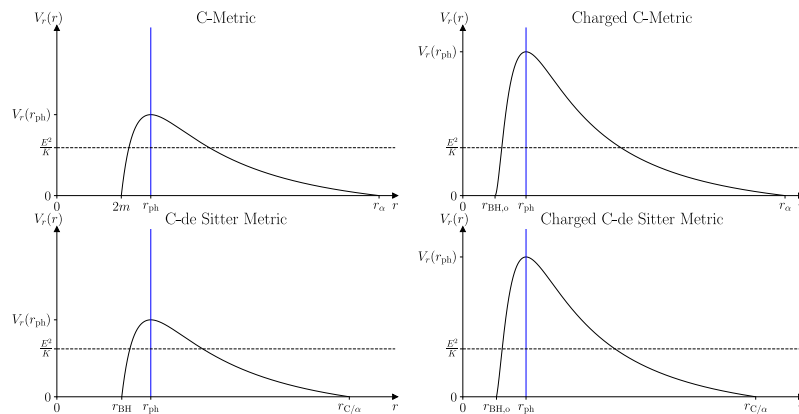


Fig. 2. Potential $V_r(r)$ of the r motion in the C-metric (top left), the charged C-metric (top right), the C-de Sitter metric (bottom left) and the charged C-de Sitter metric (bottom right) for $\Lambda = 1/(200m^2)$, $e = m$, and $\alpha = 1/(10m)$. The axes have the same scale in all four plots.

We begin with discussing the r motion. Following Ref. 13 we first rewrite (6) in terms of the potential $V_r(r)$

$$\frac{1}{r^4 K} \left(\frac{dr}{d\lambda} \right)^2 + V_r(r) = \frac{E^2}{K}, \quad (10)$$

where

$$V_r(r) = \left(\frac{1}{r^2} - \alpha^2 \right) \left(1 - \frac{2m}{r} + \frac{e^2}{r^2} \right) - \frac{\Lambda}{3}. \quad (11)$$

Fig. 2 shows the potentials for the C-metric (top left), the charged C-metric (top right), the C-de Sitter metric (bottom left) and the charged C-de Sitter metric (bottom right). For all four metrics the potential has a similar structure. The most striking difference occurs close to the (outer) black hole horizon. For $e \neq 0$ the maximum of $V_r(r)$ is much higher than in the uncharged case. In addition for $\Lambda > 0$ $V_r(r)$ approaches zero at a smaller radius coordinate $r_{C/\alpha} < r_\alpha$. The maximum of the potential at $E^2/K = V_r(r_{\text{ph}})$ marks the radius coordinate of an unstable photon sphere. We can calculate the radius coordinate of the photon sphere by calculating $dr/d\lambda = d^2r/d\lambda^2 = 0$. Combining both conditions leads to the determining equation

$$r^3 + \frac{1 - \alpha^2 e^2}{m\alpha^2} r^2 - \frac{3}{\alpha^2} r + \frac{2e^2}{m\alpha^2} = 0 \quad (12)$$

for the radius of the photon sphere r_{ph} . It is remarkable that although the spherical symmetry is broken by the acceleration parameter the cosmological constant does not have any effect on the radius coordinate of the photon sphere. The roots of this equation can be analytically obtained using Cardano's method. As long as $e^2 < 1/\alpha^2$ we get three real solutions. Only the largest root lies in the region of outer communication $r_{\text{BH},o} < r < r_{C/\alpha}$ and thus marks the position of the photon sphere. When $e = 0$ the polynomial reduces to second order and r_{ph} is given by^{12,13}

$$r_{\text{ph}} = \frac{6m}{1 + \sqrt{1 + 12\alpha^2 m^2}}. \quad (13)$$

We can read from Fig. 2 that at r_{ph} $V_r(r_{\text{ph}})$ has always a maximum and thus orbits of geodesics on the photon sphere are unstable. Here, unstable means that if the orbit of a lightlike geodesic on the photon sphere was radially infinitesimally perturbed the light ray would either fall into the black hole or escape to (conformal) infinity. Using the potential we can distinguish three different types of lightlike motion. For $E^2/K > V_r(r_{\text{ph}})$ lightlike geodesics have no turning points. Here we have to distinguish between the cases $K = 0$ (we will see in Section 3.3 that these geodesics are principal null geodesics) and $K > 0$. For $E^2/K > V_r(r_{\text{ph}})$ and $K = 0$ (6) was already solved in Ref. 13. In this case the solution reads:

$$r(\lambda) = \frac{r_i}{1 - i_{r_i} r_i E (\lambda - \lambda_i)}, \quad (14)$$

where $i_{r_i} = \text{sgn}(dr/d\lambda|_{r=r_i})$. In the case $E^2/K > V_r(r_{\text{ph}})$ and $K > 0$ (6) has two real and two complex conjugated roots. We label them such that $r_1 > r_2$ and $r_3 = \bar{r}_4 = R_3 + iR_4$. To solve (6) we now substitute^{17,18}

$$r = \frac{r_1 \bar{R} - r_2 R + (r_1 \bar{R} + r_2 R) \cos \chi_r}{\bar{R} - R + (\bar{R} + R) \cos \chi_r}, \quad (15)$$

8

where

$$R = \sqrt{(R_3 - r_1)^2 + R_4^2} \quad \text{and} \quad \bar{R} = \sqrt{(R_3 - r_2)^2 + R_4^2}. \quad (16)$$

Then we follow the steps described in Appendix B of Ref. 13 and obtain the solution in terms of Jacobi's elliptic cn function. It reads

$$r(\lambda) = \frac{r_1 \bar{R} - r_2 R + (r_1 \bar{R} + r_2 R) \text{cn}(a_r(\lambda - \lambda_i) + \lambda_{r_i, k_1}, k_1)}{\bar{R} - R + (\bar{R} + R) \text{cn}(a_r(\lambda - \lambda_i) + \lambda_{r_i, k_1}, k_1)}, \quad (17)$$

where

$$a_r = i_{r_i} \sqrt{\left(E^2 + \left(\alpha^2 + \frac{\Lambda}{3}\right) K\right) R \bar{R}}, \quad \lambda_{r_i, k_1} = F_L(\chi_{r_i}, k_1), \quad (18)$$

$$\chi_{r_i} = \arccos\left(\frac{(r_i - r_2)R - (r_i - r_1)\bar{R}}{(r_i - r_2)R + (r_i - r_1)\bar{R}}\right), \quad k_1 = \frac{(R + \bar{R})^2 - (r_1 - r_2)^2}{4R\bar{R}}.$$

The condition $E^2/K = V_r(r_{\text{ph}})$ characterises lightlike geodesics asymptotically coming from or going to the photon sphere. In this case (6) has four real roots, two of which are equal. We label them such that $r_1 = r_2 = r_{\text{ph}} > r_3 > r_4$. In this case we substitute

$$r = r_3 + \frac{3a_{3,r}}{12y - a_{2,r}}, \quad (19)$$

where

$$a_{2,r} = 6 \left(E^2 + \left(\alpha^2 + \frac{\Lambda}{3}\right) K\right) r_3^2 - 6m\alpha^2 K r_3 - (1 - \alpha^2 e^2) K, \quad (20)$$

$$a_{3,r} = 4 \left(E^2 + \left(\alpha^2 + \frac{\Lambda}{3}\right) K\right) r_3^3 - 6m\alpha^2 K r_3^2 - 2(1 - \alpha^2 e^2) K r_3 + 2mK. \quad (21)$$

Then we follow the steps described in Section 3.2.3 in Ref. 13 and obtain as solution for $r(\lambda)$:

$$r(\lambda) = r_3 - \frac{(r_{\text{ph}} - r_3)(r_3 - r_4)}{r_{\text{ph}} - r_3 - (r_{\text{ph}} - r_4) \tanh^2\left(b_r + i_{r_i} \sqrt{\frac{a_{3,r}(r_{\text{ph}} - r_4)}{4(r_{\text{ph}} - r_3)(r_3 - r_4)}}(\lambda_i - \lambda)\right)}, \quad (22)$$

where

$$b_r = \text{artanh}\left(\sqrt{\frac{(r_i - r_4)(r_{\text{ph}} - r_3)}{(r_i - r_3)(r_{\text{ph}} - r_4)}}\right). \quad (23)$$

All remaining lightlike geodesics have $E^2/K < V_r(r_{\text{ph}})$. These geodesics have four real roots and can pass through a turning point. Outside the photon sphere this turning point is always a minimum. For solving (6) we now label the roots such that $r_1 = r_{\text{min}} > r_2 > r_3 > r_4$. Then we substitute^{17,18}

$$r = r_2 + \frac{(r_1 - r_2)(r_2 - r_4)}{r_2 - r_4 - (r_1 - r_4) \sin^2 \chi_r}. \quad (24)$$

Again we apply the steps described in Appendix B of Ref. 13. This time we obtain the solution to (6) in terms of Jacobi's elliptic sn function

$$r(\lambda) = r_2 + \frac{(r_1 - r_2)(r_2 - r_4)}{r_2 - r_4 - (r_1 - r_4)\text{sn}^2(c_r(\lambda - \lambda_i) + \lambda_{r_i, k_2}, k_2)}, \quad (25)$$

where

$$c_r = \frac{i_{r_i}}{2} \sqrt{\left(E^2 + \left(\alpha^2 + \frac{\Lambda}{3}\right) K\right) (r_1 - r_3)(r_2 - r_4)}, \quad \lambda_{r_i, k_2} = F_L(\chi_{r_i}, k_2), \quad (26)$$

$$\chi_{r_i} = \arcsin\left(\sqrt{\frac{(r_i - r_1)(r_2 - r_4)}{(r_i - r_2)(r_1 - r_4)}}\right), \quad k_2 = \frac{(r_2 - r_3)(r_1 - r_4)}{(r_1 - r_3)(r_2 - r_4)}.$$

3.2. The t Coordinate

Now we calculate the time coordinate t . The right-hand side of (5) depends only on $r(\lambda)$. Therefore, we first rewrite (5) as a differential of r . For this purpose we divide (5) by the root of (6). Then we integrate over r starting at $t(\lambda_i) = t(r_i) = t_i$. The resulting integral reads

$$t(\lambda) = t_i + \int_{r_i \dots}^{\dots r(\lambda)} \frac{E r'^2 dr'}{Q(r') \sqrt{E^2 r'^4 - r'^2 Q(r') K}}. \quad (27)$$

Here, we have to choose the sign of the root in accordance with the r motion and the dots in the limits of the integration indicate that we have to split the integral at the turning points. The procedure to integrate (27) is straight forward. We have to distinguish the same types of motion as for $r(\lambda)$ in Section 3.1. First we perform a partial fraction decomposition of $r'^2/Q(r')$. Then we follow the procedure described in Refs. 13 and 17 to express (27) in terms of elementary functions and elliptic integrals. Note that some of the elliptic integrals cannot immediately be expressed in form of elementary functions and elliptic integrals of first, second and third kind. However, we can easily rewrite them using the procedures described in Appendix B in Ref. 17 and Appendix A in Ref. 13.

3.3. The ϑ Motion

Again we start by rewriting (7) in terms of the potential $V_\vartheta(\vartheta)$

$$\frac{\sin^2 \vartheta}{K} \left(\frac{d\vartheta}{d\lambda}\right)^2 + V_\vartheta(\vartheta) = -\frac{L_z^2}{K}, \quad (28)$$

where

$$V_\vartheta(\vartheta) = -\sin^2 \vartheta (1 - 2\alpha m \cos \vartheta + \alpha^2 e^2 \cos^2 \vartheta). \quad (29)$$

Fig. 3 shows the potentials $V_\vartheta(\vartheta)$ of the ϑ motion for the C-(de Sitter) metric (left) and the charged C-(de Sitter) metric (right). Although in the right plot we set $e = m$ the differences are invisibly small. The potential has always a minimum at a

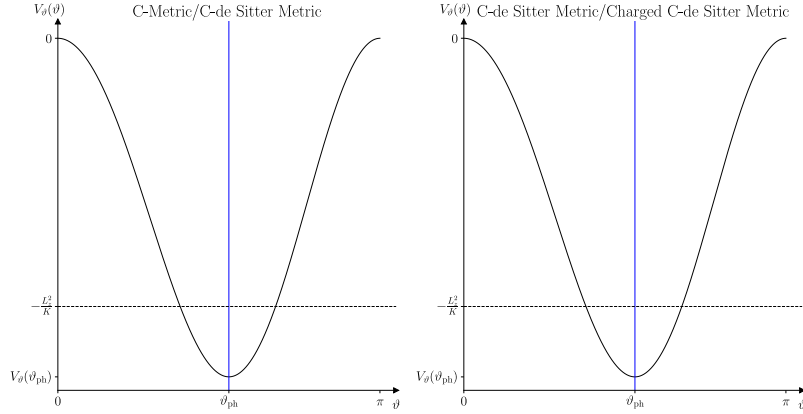


Fig. 3. Potential $V_\vartheta(\vartheta)$ of the ϑ motion in the C-metric/C-de Sitter metric (left) and the charged C-metric/C-de Sitter metric (right) for $e = m$ and $\alpha = 1/(10m)$. The axes have the same scale in both plots.

single value ϑ . At this minimum we have $d\vartheta/d\lambda = d^2\vartheta/d\lambda^2 = 0$. Combining both conditions leads to the determining equation

$$\cos^3 \vartheta - \frac{3m}{2\alpha e^2} \cos^2 \vartheta + \frac{1 - \alpha^2 e^2}{2\alpha^2 e^2} \cos \vartheta + \frac{m}{2\alpha e^2} = 0. \quad (30)$$

We determine the roots of this equation using Cardano's method. Within the permissible range $0 \leq \vartheta \leq \pi$ the equation has exactly one real root ϑ_{ph} . This is the photon cone of the charged C-(de Sitter) metric. Note that we cannot determine the limits $e \rightarrow 0$ or $\alpha \rightarrow 0$ from the calculated ϑ_{ph} directly. When we approach these limits we see that for $e \rightarrow 0$ ϑ_{ph} reduces to^{12,13}

$$\vartheta_{\text{ph}} = \arccos \left(\frac{-2\alpha m}{1 + \sqrt{1 + 12\alpha^2 m^2}} \right) \quad (31)$$

and for $\alpha \rightarrow 0$ it reduces to $\vartheta_{\text{ph}} = \pi/2$. The photon cone is unstable. Here unstable means that when light rays on the photon cone are infinitesimally perturbed in ϑ direction they will begin to oscillate between a minimum ϑ_{min} and a maximum ϑ_{max} . Based on the potential $V_\vartheta(\vartheta)$ we can distinguish two different types of motion. From (7) we can immediately read that we have $L_z = 0$ when $K = 0$ and the right-hand side of (7) vanishes. Because $L_z = 0$ implies $d\varphi/d\lambda = 0$ these are the already in Section 3.1 mentioned principal null geodesics. Also for lightlike geodesics on the photon cone ($-L_z^2/K = V_\vartheta(\vartheta_{\text{ph}})$) the right-hand side of (7) vanishes because we have two coinciding roots at $x = \cos \vartheta_{\text{ph}}$. Thus for principal null geodesics and lightlike geodesics on the photon cone the solution to (7) reads $\vartheta(\lambda) = \vartheta_i$. For all other lightlike geodesics we have $-L_z^2/K \neq V_\vartheta(\vartheta_{\text{ph}})$. These geodesics oscillate between a minimum ϑ_{min} and a maximum ϑ_{max} and each geodesic can potentially

have arbitrary many turning points. In this case we first rewrite (7) in terms of $x = \cos \vartheta$. It is easy to see that in the new parameterisation (7) reduces to a polynomial of third order in x when $e = 0$. This case was already treated in Ref. 13 and thus we do not reproduce it here. For $e \neq 0$ we always have two turning points, however, depending on the choice of L_z and K the right-hand side of (7) has two different root structures. In the first case two of the roots are real. We label them such that $x_2 = \cos \vartheta_{\max} < x_1 = \cos \vartheta_{\min}$. The other two roots are complex conjugated and we label them as $x_3 = \bar{x}_4 = X_3 + iX_4$. As first step to solve (7) we now substitute¹⁸

$$x = \frac{x_1 \bar{X} + x_2 X + (x_1 \bar{X} - x_2 X) \cos \chi_\vartheta}{\bar{X} + X + (\bar{X} - X) \cos \chi_\vartheta}, \quad (32)$$

where X and \bar{X} are given by (16). In the second step we again follow the steps described in Appendix B of Ref. 13. We obtain $\vartheta(\lambda)$ in terms of Jacobi's elliptic cn function. It reads

$$\vartheta(\lambda) = \arccos \left(\frac{x_1 \bar{X} + x_2 X + (x_1 \bar{X} - x_2 X) \text{cn}(a_\vartheta(\lambda - \lambda_i) + \lambda_{\vartheta_i, k_3}, k_3)}{\bar{X} + X + (\bar{X} - X) \text{cn}(a_\vartheta(\lambda - \lambda_i) + \lambda_{\vartheta_i, k_3}, k_3)} \right), \quad (33)$$

where $i_{\vartheta_i} = \text{sgn}(d\vartheta/d\lambda|_{\vartheta=\vartheta_i})$ and

$$a_\vartheta = i_{\vartheta_i} \sqrt{\alpha^2 e^2 K X \bar{X}}, \quad \lambda_{\vartheta_i, k_3} = F_L(\chi_{\vartheta_i}, k_3), \quad (34)$$

$$\chi_{\vartheta_i} = \arccos \left(\frac{(\cos \vartheta_i - x_1) \bar{X} + (\cos \vartheta_i - x_2) X}{(x_1 - \cos \vartheta_i) \bar{X} + (x_2 - \cos \vartheta_i) X} \right), \quad k_3 = \frac{(x_1 - x_2)^2 - (X - \bar{X})^2}{4X\bar{X}}.$$

In the second case all four roots are real and we label them such that $x_4 = \cos \vartheta_{\max} < x_3 = \cos \vartheta_{\min} < x_2 < x_1$. In this case we substitute¹⁸

$$x = x_1 - \frac{(x_1 - x_3)(x_1 - x_4)}{x_1 - x_3 + (x_3 - x_4) \sin^2 \chi_\vartheta}. \quad (35)$$

We again follow the steps described in Appendix B of Ref. 13. This time we obtain $\vartheta(\lambda)$ in terms of Jacobi's elliptic sn function

$$\vartheta(\lambda) = \arccos \left(x_1 - \frac{(x_1 - x_3)(x_1 - x_4)}{x_1 - x_3 + (x_3 - x_4) \text{sn}^2(b_\vartheta(\lambda_i - \lambda) + \lambda_{\vartheta_i, k_4}, k_4)} \right), \quad (36)$$

where

$$b_\vartheta = \frac{i_{\vartheta_i}}{2} \sqrt{\alpha^2 e^2 K (x_1 - x_3)(x_2 - x_4)}, \quad \lambda_{\vartheta_i, k_4} = F_L(\chi_{\vartheta_i}, k_4) \quad (37)$$

$$\chi_{\vartheta_i} = \arcsin \left(\sqrt{\frac{(\cos \vartheta_i - x_4)(x_1 - x_3)}{(x_1 - \cos \vartheta_i)(x_3 - x_4)}} \right), \quad k_4 = \frac{(x_1 - x_2)(x_3 - x_4)}{(x_1 - x_3)(x_2 - x_4)}.$$

3.4. The φ Motion

The φ motion is governed by (8). We immediately read that for $L_z = 0$ the right-hand side vanishes. For $K = 0$ these are the principal null geodesics. In this case we obtain the solution to (8) as $\varphi(\lambda) = \varphi_i$. If $K \neq 0$ these are geodesics crossing the

axes. What happens to these geodesics now depends on whether we assume that the string and the strut are opaque or transparent. In the former case the lightlike geodesics terminate at the string and we observe it as a black line blocking out all light emitted by sources located behind it. In the latter case the lightlike geodesics pass through the string. To see what happens when a lightlike geodesic passes through the axes we consider a series of lightlike geodesics continually approaching the axes for $L_z > 0$ and $L_z < 0$.¹³ We observe that for $L_z > 0$ and $L_z < 0$ the φ coordinate has different limits. Hence geodesics crossing the axes have two different continuations and the φ coordinate is not continuous.

Next we turn to lightlike geodesics with a double root at $x = \cos \vartheta_{\text{ph}}$ ($-L_z^2/K = V_{\vartheta}(\vartheta_{\text{ph}})$). These are lightlike geodesics on the photon cone with $\vartheta(\lambda) = \vartheta_{\text{ph}}$. In this case the right-hand side of (8) is constant and the solution $\varphi(\lambda)$ reads

$$\varphi(\lambda) = \varphi_i + \frac{L_z(\lambda - \lambda_i)}{\sin^2 \vartheta_{\text{ph}} P(\vartheta_{\text{ph}})}. \quad (38)$$

Last we turn to lightlike geodesics with $-L_z^2/K \neq V_{\vartheta}(\vartheta_{\text{ph}})$. In this case we want to express $\varphi(\lambda)$ in terms of elementary functions and elliptic integrals. For this purpose we first substitute $x = \cos \vartheta$ in (7) and (8). Then we divide (8) by the root of (7) and integrate. Now $\varphi(\lambda)$ reads

$$\varphi(\lambda) = \varphi_i + \int_{\cos \vartheta_i \dots}^{\dots \cos \vartheta(\lambda)} \frac{L_z dx'}{(1 - x'^2)P(x')\sqrt{(1 - x'^2)P(x')K - L_z^2}}. \quad (39)$$

Here, we have to choose the sign of the root such that it corresponds to the sign of the $\cos \vartheta$ motion and the dots in the limits indicate that we have to split the integral at the turning points. Again we rewrite the elliptic integral using elementary functions and the canonical forms of the elliptic integrals. For this purpose we now perform a partial fraction decomposition of $(1 - x^2)^{-1}P(x)^{-1}$. Then we use (41) in Ref. 13 and (32) and (35) to rewrite (39) in terms of elementary functions and elliptic integrals of first, second and third kind. Note that we again encounter elliptic integrals which do not immediately have a canonical form. Again we rewrite them using the procedures described in Appendix B in Ref. 17 and Appendix A in Ref. 13 (although here we have $n^2/(n^2 - 1) < 1$ and not $1 < n^2/(n^2 - 1)$ the basic integration procedure is the same).

4. Gravitational Lensing

4.1. Celestial Sphere

In astronomy the position of a light source on the sky is identified using latitude and longitude coordinates. For this purpose astronomers fix the main target of their observation at the centre of their image and measure the position of all other objects relative to the centre. In our discussion of gravitational lensing in the charged C-de Sitter metric we follow this approach. For this purpose we first fix an observer at coordinates $(x_O^\mu) = (t_O, r_O, \vartheta_O, \varphi_O)$ in the region of outer communication between

photon sphere and cosmological/acceleration horizon. Then we choose the black hole as main target of our observation and introduce an orthonormal tetrad following Refs. 8 and 13:

$$\begin{aligned} e_0 &= \frac{\Omega(r, \vartheta)}{\sqrt{Q(r)}} \partial_t \Big|_{(x_O^\mu)}, & e_1 &= \frac{\Omega(r, \vartheta) \sqrt{P(\vartheta)}}{r} \partial_\vartheta \Big|_{(x_O^\mu)}, \\ e_2 &= - \frac{\Omega(r, \vartheta)}{r \sin \vartheta \sqrt{P(\vartheta)}} \partial_\varphi \Big|_{(x_O^\mu)}, & e_3 &= - \Omega(r, \vartheta) \sqrt{Q(r)} \partial_r \Big|_{(x_O^\mu)}. \end{aligned} \quad (40)$$

We will call the angles on the celestial sphere surrounding the observer Σ (latitude) and Ψ (longitude). The angle Σ is measured from the axis along e_3 connecting lens and observer and the angle Ψ is measured in the direction of e_2 from the axis along the direction of e_1 .

Before we can investigate gravitational lensing in the charged C-de Sitter metric we first have to derive the relations between the constants of motion E , L_z and K and the angles on the observer's celestial sphere Σ and Ψ . For this purpose we consider a lightlike geodesic ending at the position of the observer. Now we first write down the tangent vector to this geodesic. It reads

$$\frac{d\eta}{d\lambda} = \frac{dt}{d\lambda} \partial_t + \frac{dr}{d\lambda} \partial_r + \frac{d\vartheta}{d\lambda} \partial_\vartheta + \frac{d\varphi}{d\lambda} \partial_\varphi. \quad (41)$$

At the position of the observer we can also express the tangent vector of the geodesic by the angles on the observer's celestial sphere and the tetrad vectors e_0 , e_1 , e_2 and e_3

$$\frac{d\eta}{d\lambda} = \sigma (-e_0 + \sin \Sigma \cos \Psi e_1 + \sin \Sigma \sin \Psi e_2 + \cos \Sigma e_3), \quad (42)$$

where σ is a normalisation constant

$$\sigma = g \left(\frac{d\eta}{d\lambda}, e_0 \right). \quad (43)$$

In our convention we have $E > 0$ and thus σ has to be negative. Because the Mino parameter λ is defined up to an affine transformation without loss of generality we can choose $\sigma = -r_O^2 / \Omega(r_O, \vartheta_O)^2$.¹³ Now we insert σ in (42) and (43). Then a comparison of the coefficients of (41) and (42) leads to¹³

$$E = \frac{\sqrt{Q(r_O)}}{\Omega(r_O, \vartheta_O)}, \quad L_z = \frac{r_O \sqrt{P(\vartheta_O)} \sin \vartheta_O \sin \Sigma \sin \Psi}{\Omega(r_O, \vartheta_O)}, \quad K = \frac{r_O^2 \sin^2 \Sigma}{\Omega(r_O, \vartheta_O)^2}. \quad (44)$$

4.2. Angular Radius of the Photon Sphere

The shadow of a black hole is a highly idealised concept. It is constructed as follows. First we place an observer in the region of outer communication between photon sphere and cosmological/acceleration horizon. Then we distribute light sources everywhere except between observer and the black hole. Therefore the former region

is associated with brightness on the observer's sky while the latter is associated with darkness. Now we shoot back light rays exactly on the boundary between these areas of brightness and darkness. These are geodesics asymptotically going to the photon sphere. They have the same constants of motion as light rays on the photon sphere and thus a double root at r_{ph} . We now use this fact to calculate the angular radius of the shadow. For this purpose we first insert (44) in (6). Then we employ that $dr/d\lambda|_{r=r_{\text{ph}}} = 0$. Now we solve for Σ and get as angular radius of the shadow¹³

$$\Sigma_{\text{ph}} = \arcsin \left(\frac{r_{\text{ph}}}{r_O} \sqrt{\frac{Q(r_O)}{Q(r_{\text{ph}})}} \right). \quad (45)$$

4.3. Lens Map

The lens map or lens equation maps images on the observer's sky back to the source surface. This article is an extension of the work presented in Ref. 13 and therefore we will closely follow their definition of the lens map. To set up the lens map we first distribute light sources on a sphere with radius $r_O < r_L$ in the region of outer communication. Then we shoot light rays backwards in time from the position of the observer (x_O^μ). Some of the light rays, but not all, will intersect with the sphere of light sources. These geodesics form a map from the celestial sphere of the observer to the sphere of light sources

$$(\Sigma, \Psi) \rightarrow (\vartheta_L(\Sigma, \Psi), \varphi_L(\Sigma, \Psi)). \quad (46)$$

This is our lens equation. Now we have to calculate $\vartheta_L(\Sigma, \Psi)$ and $\varphi_L(\Sigma, \Psi)$ to obtain the lens map for the charged C-de Sitter metric. For this purpose we set $(x_i^\mu) = (x_O^\mu)$ and insert (44) into the solutions of the equations of motion derived in Section 3. Due to the symmetry of the charged C-de Sitter metric we can choose t_O and φ_O arbitrarily. Similarly λ is only defined up to an affine transformation. Therefore, to ease all following calculations we choose them such that $\lambda_O = 0$, $t_O = 0$ and $\varphi_O = 0$.

As first step towards calculating $\vartheta_L(\Sigma, \Psi)$ and $\varphi_L(\Sigma, \Psi)$ we calculate the Mino parameter $\lambda_L < \lambda_O$

$$\lambda_L = \int_{r_O \dots}^{\dots r_L} \frac{\Omega(r_O, \vartheta_O) dr'}{\sqrt{Q(r_O) r'^4 - r_O^2 \sin^2 \Sigma r'^2 Q(r')}}. \quad (47)$$

Again for lightlike geodesics passing through a turning point we have to split the integral and choose the sign of the root in the denominator in agreement with the r motion. Now we insert λ_L in the appropriate solution for $\vartheta(\lambda)$ in Section 3.3 and obtain $\vartheta_L(\Sigma, \Psi)$. Next we count the number of turning points n of the ϑ motion. For this purpose we calculate the Mino parameter up to the first turning point of the ϑ motion λ_0 . In the next step we calculate the difference of the Mino parameter between two subsequent turning points of the ϑ motion $\Delta\lambda$. Now we count how many turning points occur while $\lambda_L < \lambda_n = \lambda_0 + n\Delta\lambda$. Finally we

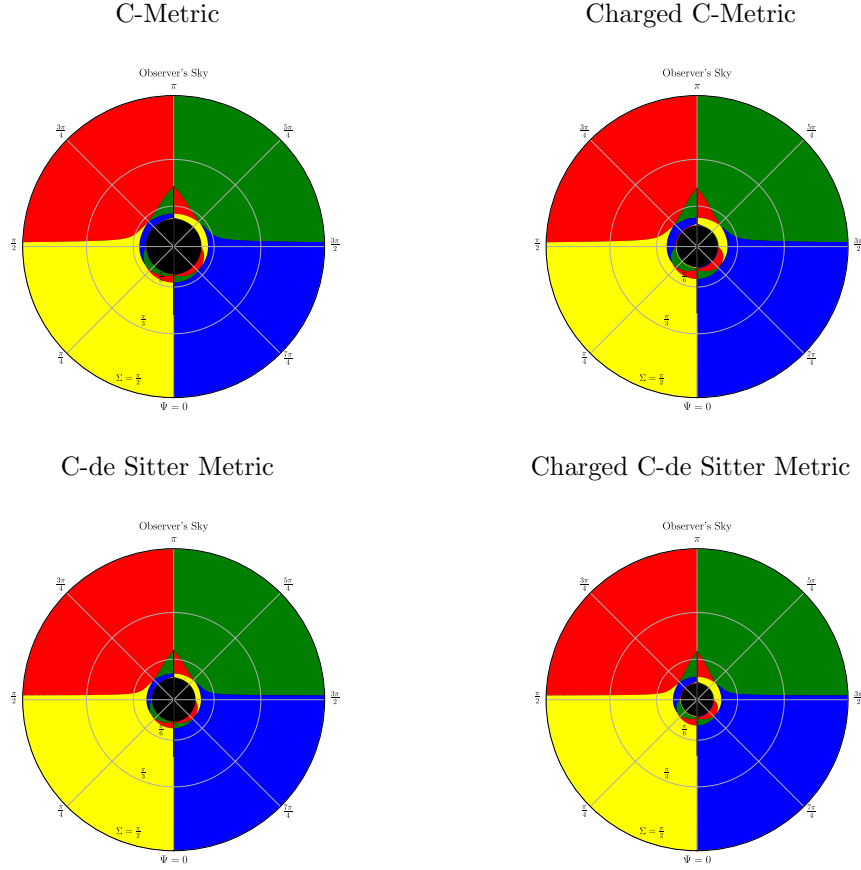


Fig. 4. Lens equation for the C-metric¹³ (top left), the charged C-metric (top right), the C-de Sitter metric (bottom left) and the charged C-de Sitter metric (bottom right) for $\Lambda = 1/(200m^2)$, $e = m$ and $\alpha = 1/(10m)$. The observer is located at $r_O = 8m$, $\vartheta_O = \pi/2$ and the sphere of light sources is located at $r_L = 9m$. The colour convention follows Refs. 13 and 14 and is as follows: $0 \leq \vartheta_L \leq \pi/2$: red/green; $\pi/2 < \vartheta_L \leq \pi$: yellow/blue $0 \leq \varphi_L < \pi$: green/blue; $\pi \leq \varphi_L < 2\pi$: red/yellow. The black lines at $\Psi = 0$ and $\Psi = \pi$ mark light rays that cross the axes at least once.

calculate $\varphi_L(\Sigma, \Psi)$ from (39) as described in Section 3.4.

Fig. 4 shows plots of the lens equation in stereographic projection for the C-metric (top left), the charged C-metric (top right), the C-de Sitter metric (bottom left) and the charged C-de Sitter metric (bottom right) for $\Lambda = 1/(200m^2)$, $e = m$ and $\alpha = 1/(10m)$. The observer is located at $r_O = 8m$ and $\vartheta_O = \pi/2$. The sphere of light sources is located at $r_L = 9m$. The black lines at $\Psi = 0$ and $\Psi = \pi$ mark lightlike geodesics that cross the string or the strut at least once. The black circle in the centre of each image is the shadow of the black hole. The images clearly show that the angular radius Σ_{ph} of the shadow decreases when $0 < \Lambda$ and $0 < e$. All four images basically show the same features up to a scaling. The symmetry

with respect to $\Psi = \pi/2$ and $\Psi = 3\pi/2$ is clearly broken. Thus in all four cases light rays ending parallel to the surface $\vartheta = \pi/2$ generally come from light sources not located at $\vartheta = \pi/2$. However, the shape of the features shown in the images is clearly symmetric with respect to the line marked by $\Psi = 0$ and $\Psi = \pi$. On the right side of the line of symmetry at the outer boundary of each image we first have a region coloured in blue and green. In this region we find images where the covered angle $0 < \Delta\varphi < \pi$. These are images of first order. Adjacent to these images, closer to the shadow we find a region coloured in yellow and red. In this region we find images for which the light ray covered the angle $\pi < \Delta\varphi < 2\pi$. These are images of second order. If we go closer to the shadow we also find images of third and fourth order. The boundaries between the images of different orders mark the positions of the critical curves. On the left side of the line of symmetry we find the same features, however, the ordering of the colours is reversed. In addition we observe that at $\Psi = \pi$ images of second order already occur further away from the shadow than for $\Psi = 0$. This implies that light rays passing close to the string cover the same angle $\Delta\varphi$ faster than light rays passing close to the strut.

4.4. Redshift

The redshift z of a light ray relates its energy at the time of emission by a light source to its energy at the position at which it is detected by an observer. It is directly accessible to observation via the frequency shift of atomic or molecular absorption lines. We will now construct redshift maps. For this purpose we will use the same settings and results we obtained from constructing the lens map in Section 4.3. In this setting observer and light source are static and the corresponding general redshift formula can be found in Ref. 19, pp. 45. After inserting the metric coefficients g_{tt} of the charged C-de Sitter metric it reads¹³

$$z = \sqrt{\frac{g_{tt}|_{x_O}}{g_{tt}|_{x_L}}} - 1 = \sqrt{\frac{Q(r_O)}{Q(r_L)} \frac{\Omega(r_L, \vartheta_L(\Sigma, \Psi))}{\Omega(r_O, \vartheta_O)}} - 1. \quad (48)$$

Fig. 5 shows plots of the redshift maps for the same observer-source geometry as for the lens maps in Fig. 4. In all four plots the outer region is dominated by redshifts. The redshift has two maxima around $\Psi = \pi$ and at $\Psi = 0$ (close to the shadow). In addition in all images we observe a region of blueshifts centered around $\Psi = 0$. Another crescent shaped region of blueshifts can be found at $\Psi = \pi$ close to the shadow. What are now the effects of the cosmological constant Λ and the electric charge e ? Comparing the images with $\Lambda = 0$ in the upper row with the images with $\Lambda = 1/(200m^2)$ in the lower row shows that when we turn on the cosmological constant the redshift range shifts from $-1 < z < 2$ to $-0.8 < z < 6$, respectively. The two blueshift areas move to lower latitudes closer to the centre of the shadow. In addition the fraction of the images covered by blueshifts decreases. The effects of the electric charge e are less strongly pronounced. When we compare the images on the left ($e = 0$) to the images on the right ($e = m$) we observe that in the top

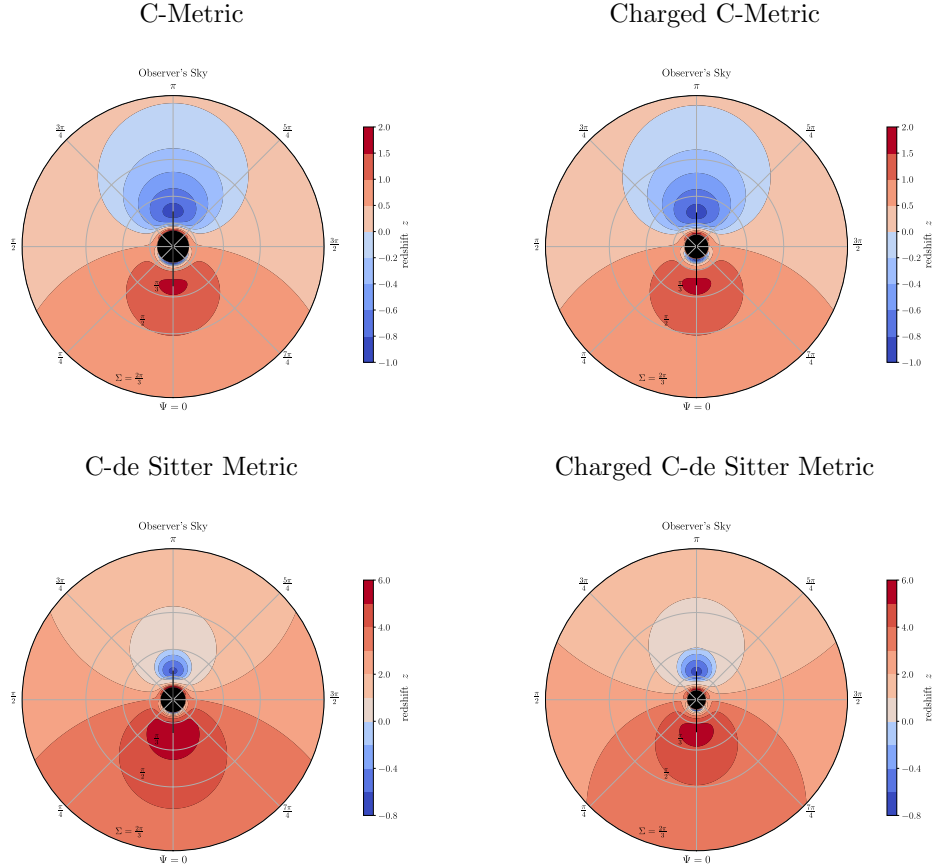


Fig. 5. Redshift maps for the C-metric¹³ (top left), the charged C-metric (top right), the C-de Sitter metric (bottom left) and the charged C-de Sitter metric (bottom right) for $\Lambda = 1/(200m^2)$, $e = m$ and $\alpha = 1/(10m)$. The observer is located at $r_O = 8m$, $\vartheta_O = \pi/2$ and the sphere of light sources is located at $r_L = 9m$. The black lines at $\Psi = 0$ and $\Psi = \pi$ mark light rays that cross the axes at least once.

row the areas with blueshift move to slightly lower latitudes while they still seem to cover roughly the same fraction of the image. However, comparing both images in the lower row indicates that in the presence of a cosmological constant turning on the electric charge leads to an increase of the fraction of the image covered by blueshifts. In addition the areas of blueshifts shift to lower latitudes but appear to be located at angular distances further away from the shadow.

4.5. Travel Time

The travel time $T = t_O - t_L$ measures in terms of the time coordinate t the elapsed time between the emission of a light ray by a source at a time t_L and the detection

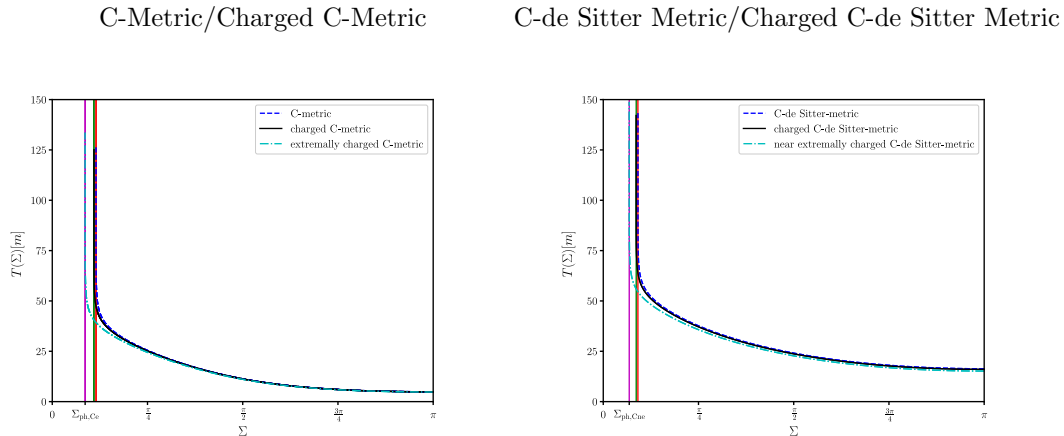


Fig. 6. Travel time $T(\Sigma)$ for the C-metric and the charged C-metric (left), and the C-de Sitter metric and the charged C-de Sitter metric (right) for $\Lambda = 1/(200m^2)$, $e = m$ in the extremal and near extremal case, otherwise $e = m/2$ and $\alpha = 1/(10m)$. The observer is located at $r_O = 8m$ and the sphere of light sources is located at $r_L = 9m$. $\Sigma_{\text{ph,Ce}}$ and $\Sigma_{\text{ph,Cne}}$ mark the position of the angular radius of the shadow on the observer's celestial sphere for the extremally charged C-metric and the near extremally charged C-de Sitter metric, respectively.

of the same light ray by an observer at the time t_O . We obtain the travel time integral by inserting (44) and $t_O = 0$ in (27). We evaluate the travel time as described in Section 3.2. Fig. 6 shows the travel time for the (charged) C-metric (left) and the (charged) C-de Sitter metric (right) for $\Lambda = 1/(200m^2)$, $e = m/2$ in the regular case, $e = m$ in the (near) extremal case and $\alpha = 1/(10m)$. The observer is located at $r_O = 8m$ and the light source is located at $r_L = 9m$. The left plot shows that for $\Sigma > \pi/2$ in the C-metric and the charged C-metric the travel time is roughly the same. When we turn on the cosmological constant this drastically changes. In comparison to the (charged) C-metric the travel time gets significantly longer. However, turning on the electric charge in presence of a positive cosmological constant leads to a decrease of the travel time. In addition both plots indicate that for $e = m/2$ the travel time close to Σ_{ph} is slightly shorter than for $e = 0$ while it is significantly longer for $e = m$.

5. Summary and Implications for Observations

In this article we extended the work presented for the C-metric in Ref. 13 to the charged C-de Sitter metrics. In the first part we discussed and solved the equations of motion using elementary as well as elliptic functions and elliptic integrals. In the second part we used the derived analytical solutions to investigate gravitational lensing in the charged C-de Sitter metrics.

How can we now use these results in combination with observational data to distinguish between the different black hole spacetimes and in particular to measure the electric charge of a black hole?

In the charged C-de Sitter metrics the shape of the shadow is always circular. Its angular radius decreases with increasing Λ , e and α . However, because the distance between the observer on Earth and the black hole lens is not a priori known it alone cannot be used to determine the nature of the black hole. The length of the travel time in particular close to the shadow is more characteristic for each space-time. Unfortunately in real astrophysical settings (multiple imaging systems) we can only measure travel time differences leading to similar ambiguities as for the shadow. However, the charged C-de Sitter spacetimes also admit two very characteristic lensing features that distinguish them from their non-accelerating counterparts ($\alpha = 0$). The first characteristic is the breaking of symmetry with respect to the equatorial plane on the celestial sphere of the observer in the lens maps. Here, the most salient feature was the observation that images of second order occur at larger (lower) angular distance from the shadow close to the string (strut). The second characteristic is that the redshift z is a function of the coordinates on the observer's celestial sphere. The breaking of symmetry can be tested by observing multiple images from the same light source gravitationally lensed by a black hole. In such a system we can measure the position of the images on the celestial sphere of the observer relative to the lens and then compare it with theoretical predictions. Similarly although our construction of the redshift map is highly idealised we may be able to find astrophysical systems similar to this configuration. In such a system, we can measure the redshift of known emission lines and construct a partial redshift map to determine if it is a function of the coordinates on the observer's celestial sphere. Observing the symmetry breaking and showing that the measured redshift is a function on the observer's celestial sphere tells us with high certainty that the observed black hole is accelerating and can be described by one of the charged C-de Sitter metrics. However, due to the ambiguity introduced by the a-priori unknown distance between observer and black hole lens we cannot use these measurements alone to determine Λ , e and α . Therefore, to correctly identify the nature of the spacetime describing the black hole we observe, and having the chance to accurately measure the mass parameter m , the cosmological constant Λ , the electric charge e and the acceleration parameter α we need to combine high accuracy measurements of the angular diameter of the shadow, the redshift function on the observer's celestial sphere and of the position of and the travel time differences between two or more multiple images from the same source. Unfortunately even with very high accuracy observations for most black holes the electric charge e is likely to be far too low to be measured and one may only be able to estimate an upper limit.

Acknowledgments

I would like to thank Volker Perlick for the helpful discussions. I acknowledge financial support from QuantumFrontiers. I also acknowledge support from Deutsche Forschungsgemeinschaft within the Research Training Group 1620 Models of Gravity.

References

1. J. M. Corral-Santana, J. Casares, T. Muñoz-Darias, F. E. Bauer, I. G. Martínez-Pais and D. M. Russell, BlackCAT: A catalogue of stellar-mass black holes in X-ray transients, *Astron. Astrophys.* **587**, p. A61 (2016).
2. R. Abbott *et al.*, Population Properties of Compact Objects from the Second LIGO–Virgo Gravitational-Wave Transient Catalog, *Astrophys. J. Lett.* **913**, p. L7 (2021).
3. K. Gültekin, E. M. Cackett, J. M. Miller, T. Di Matteo, S. Markoff and D. O. Richstone, A CHANDRA Survey of Supermassive Black Holes with Dynamical Mass Measurements, *Astrophys. J.* **749**, p. 129 (2012).
4. GRAVITY Collaboration, Detection of the gravitational redshift in the orbit of the star S2 near the Galactic centre massive black hole, *Astron. Astrophys.* **615**, p. L15 (2018).
5. The Event Horizon Telescope Collaboration, First M87 Event Horizon Telescope Results. I. The Shadow of the Supermassive Black Hole, *Astrophys. J. Lett.* **875**, p. L1 (2019).
6. E. Castellanos, J. C. Degollado, C. Lämmerzahl, A. Macías and V. Perlick, Bose-Einstein condensates in charged black-hole spacetimes, *JCAP* **2018**, p. 043 (2018).
7. J. B. Griffiths and J. Podolský, *Exact Space-Times in Einstein's General Relativity* (Cambridge University Press, Cambridge, 2009).
8. A. Grenzebach, V. Perlick and C. Lämmerzahl, Photon regions and shadows of accelerated black holes, *Int. J. of Mod. Phys. D* **24**, p. 1542024 (2015).
9. A. Grenzebach, *The Shadow of Black Holes* Springer Briefs in Physics, Springer Briefs in Physics (Springer, Heidelberg, 2016).
10. J. F. Plebanski and M. Demianski, Rotating, Charged, and Uniformly Accelerating Mass in General Relativity, *Ann. Phys. (N. Y.)* **98**, 98 (1976).
11. M. Sharif and S. Iftikhar, Equatorial gravitational lensing by accelerating and rotating black hole with NUT parameter, *Astrophys. Space Sci.* **361**, p. 36 (2016).
12. M. Alrais Alawadi, D. Batic and M. Nowakowski, Light bending in a two black hole metric, *Class. Quantum Grav.* **38**, p. 045003 (2021).
13. T. C. Frost and V. Perlick, Lightlike geodesics and gravitational lensing in the spacetime of an accelerating black hole, *Class. Quantum Grav.* **38**, p. 085016 (2021).
14. A. Bohn, W. Thrope, F. Hébert, K. Henriksson, D. Bunandar, M. A. Scheel and N. W. Taylor, What does a binary black hole merger look like?, *Class. Quantum Grav.* **32**, p. 065002 (2015).
15. J. B. Griffiths, P. Krtouš and J. Podolský, Interpreting the C-metric, *Class. Quantum Grav.* **23**, 6745 (2006).
16. Y. Mino, Perturbative approach to an orbital evolution around a supermassive black hole, *Phys. Rev. D* **67**, p. 084027 (2003).
17. S. E. Gralla and A. Lupsasca, Null geodesics of the Kerr exterior, *Phys. Rev. D* **101**, p. 044032 (2020).
18. H. Hancock, *Elliptic Integrals* Mathematical Monographs, Mathematical Monographs, 1 edn. (New York John Wiley & Sons, 1917).
19. N. Straumann, *General Relativity* Graduate Texts in Physics, Graduate Texts in Physics, 2 edn. (Springer, Heidelberg, 2013).